USGS State of Washington Water Research Center
Project Report – Neumann (PI)

Arsenic Fate Following In-Situ Sulfate Reduction: Assessing the Sustainability of a Promising Groundwater Remediation Strategy

PROBLEM & RESEARCH OBJECTIVE

Arsenic contaminated groundwater is a global problem, negatively impacting the health of millions of people worldwide who rely on groundwater for drinking and irrigation purposes — including those who live in Washington State. A country-wide survey conducted in 2006 documented Pierce and King county as having a high risk of arsenic exposure through untreated groundwater consumption [Twarakavi and Kaluarachchi, 2006], while a state-wide survey of 107 Washington homes found 91% with detectable levels of arsenic in their water [Nielsen et al., 2010]. Chronic consumption of arsenic results in skin lesions, skin cancer, bladder cancer, and lung cancer, and has been shown to increase the rate of morbidity by 9–68% [Argos et al., 2010]. While some of the groundwater arsenic in Washington State is of geologic origin (i.e., mobilized off aquifer sediments) [Murcott, 2012], much of it is due to past industrial [Paul et al., 1996], mining [Peplow and Edmonds, 2004], and disposal [Beaulieu and Ramirez, 2013] activities.

Given the prevalence and negative health consequences of arsenic-contaminated groundwater, it is important —at both the global and local scale— to develop robust and sustainable groundwater arsenic remediation strategies. *In-situ* arsenic removal from groundwater by induced microbial sulfate reduction, either with or without the addition of zero-valent iron (ZVI), is a promising remediation strategy. It works by injecting the appropriate microbial substrates (e.g., sulfate, carbon sources, ZVI) into the subsurface, creating biogeochemical conditions that favor the formation of minerals that incorporate arsenic during precipitation or create surfaces upon which arsenic adsorbs. Such minerals include arsenic-bearing iron sulfides, arsenic sulfides, and, when ZVI is used, iron (oxy)hydroxides [O'Day et al., 2004; Lien and Wilkin, 2005]. While numerous laboratory studies have documented the ability of induced sulfate reduction to remove arsenic from solution, adoption of the technique remains low, reflecting the sparse number of field-based applications [Benner et al., 2002; Saunders et al., 2008; Wilkin et al., 2009; Beaulieu and Ramirez, 2013] and a deficiency of direct evidence regarding the arsenic sequestration mechanisms.

The objective of the proposed project was to advance understanding of the long-term sustainability of arsenic removal from groundwater following field-scale application of induced microbial sulfate reduction with and without ZVI. Washington State has one of the few field applications of induced microbial sulfate reduction. The WA Department of Ecology has overseen application of the technique (with and without ZVI) as permeable reactive barriers (PRBs) at the B&L Woodwaste site to remediate the leading edges of a groundwater arsenic plume emanating from a former woodwaste landfill near Tacoma [Beaulieu and Ramirez, 2013]. From the mid-1970s until the early 1980s, the unlined landfill received woodwaste that was contaminated with slag from the former Asarco smelter in Ruston. The Asarco slag contained up to 2% arsenic, and biogeochemical conditions formed within the base of the landfill resulted in a redox-driven release of arsenic that created a large groundwater arsenic plume with current concentrations reaching ~5,000 micrograms per liter (µg/L), or 1000x the site's background concentration of 5 µg/L. The plume endangers Hylebos Creek, a salmon-bearing waterway, and is considered a threat to human health and the environment by the Washington Department of Ecology. The applied remediation strategy with ZVI has decreased arsenic concentrations within the PRBs by 66–96%, and has maintained low arsenic concentrations over a period of ~ 2 years

(Figure 1). The remediation strategy without ZVI has had more limited success. In this treatment concentrations initially decreased but then increased again (Figure 2).

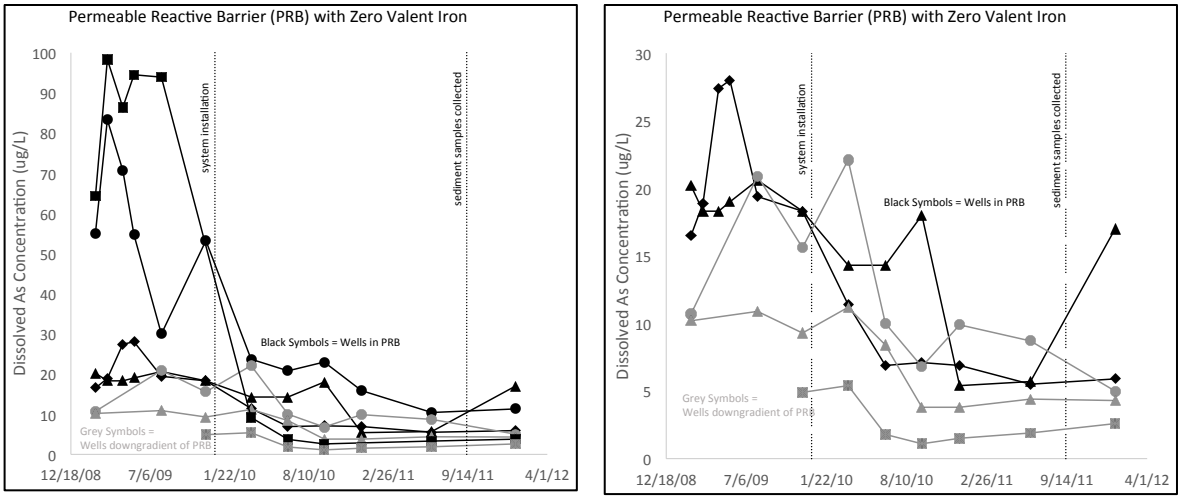

Figure 1: Arsenic concentrations in groundwater in (black symbols) and downgradient (grey symbols) of permeable reactive barrier (PRB) treated with induced sulfate reduction that included zero-valent iron. The plot on the left includes all sampled wells. The plot on the right includes only the wells with lower initial arsenic concentrations (<30 μg/L). The time points corresponding to treatment initiation (i.e., injection of treatment substrates into subsurface) and sediment sample collection for this study are marked in both plots. The plots are modified from Beaulieu and Ramierez [2013].

To achieve our objective, we worked to characterize the arsenic sequestration mechanism within the PRB's treated both with and without ZVI. Ultimately, we wanted to answer the following two questions:

- Is arsenic co-precipitated with minerals and/or adsorbed onto mineral surfaces in the two PRBs?
- What minerals are involved in removing arsenic from solution in the two PRBs?

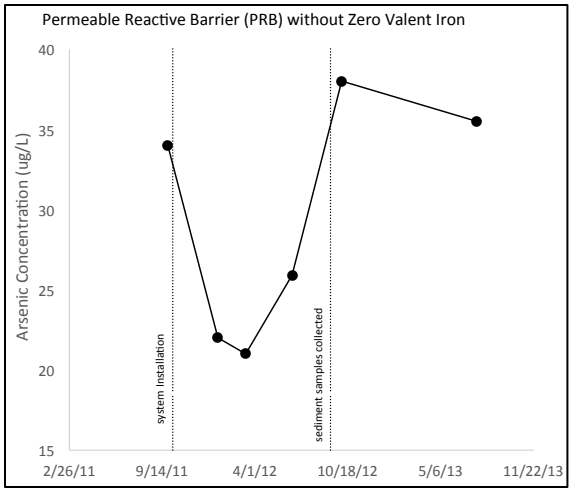

Figure 2: Arsenic concentrations in permeable reactive barrier treated with induced sulfate reduction that did not include zero-valent iron. Plot is modified from Floyd|Snider and AMEC [2013].

The arsenic sequestration mechanisms occurring during induced sulfate reduction will dictate the success and long-term stability of the treatment. For example, arsenic incorporated into minerals is generally less mobile than that adsorbed onto mineral surfaces, and arsenic associated with sulfide minerals is likely less mobile than that associated with iron (oxy)hydroxides due to the prevalence of iron-reducing conditions within natural groundwater that can promote reductive dissolution of iron (oxy)hydroxides [Han et al., 2011].

METHODOLOGY

We used x-ray adsorption spectroscopy and x-ray fluorescence to help identify the mechanisms involved with arsenic sequestration in the two PRBs. Below we discuss our

methods for collecting aquifer sediment from both PRBs, preparing the sediment for these analyses and conducting these analyses.

Sample Collection and Storage. Aquifer sediment samples were collected from the B&L Woodwaste site on September 11, 2012. Samples were collected using a direct-push drill rig at locations where induced sulfate reduction was stimulated without ZVI and with ZVI iron. Sediment was collected from depths where dissolved arsenic concentrations and hydraulic conductivity were highest, which corresponded to depths of 13.5 to 16.5 feet for the non-ZVI location, and 17 to 20 feet for the ZVI location. Samples were collected in plastic core liners and capped. Cores were put, along with oxygen-scavenging sachets (GasPak, BD Diagnostic Systems), into gas-impermeable bags that were heat-sealed in the field. Cores were stored in a cooler with dry ice. After transport back to the lab, samples were stored in the freezer.

Preparation of Aquifer Materials. One three-foot long core from each collection location (i.e., location with ZVI and without ZVI) was thawed inside an anaerobic glove box. Each core was dried inside the glove box and homogenized with an acid-washed plastic spoon in an acid-washed and furnaced (550 °C for 4 hours) glass bowl. Dried samples were sieved with a plastic #200 sieve (Model SV-165#200, Gilson Company, Inc., Lewis Center, OH) to isolate the fine fraction. The sieving step was done to concentrate the arsenic and achieve a stronger XAS signal. The sample was spread out as a single layer onto a piece of Kapton tape and sealed with additional Kapton tape to keep the sample anoxic during analysis (Figure 3). Samples were then sealed into a gas-impermeable ESCAL bag with an oxygen-scavenging sachet for transport to the synchrotron beamline.

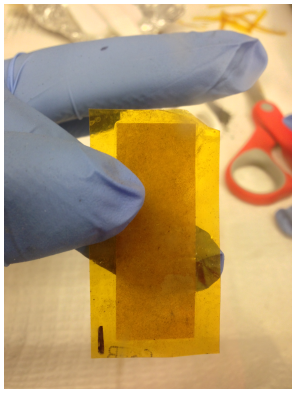

Figure 3: Aquifer sediment sample spread onto Kapton tape in preparation for synchetron analysis.

Synchrotron Measurements. We obtained direct evidence of arsenic sequestration mechanisms using microscale x-ray fluorescence (μXRF) and x-ray absorption (μXAS) capabilities at the Stanford Synchrotron Radiation Lightsource Beamline 2-3 in Menlo Park, CA. Using μXRF, we created fluorescence element composition maps, and using μXAS we collected XANES (X-ray absorption near edge structure) spectra from micron-scale points of interest within the samples to determine solid phase speciation and local coordination of arsenic [Newville, 2004]. XANES is sensitive to formal oxidation state and coordination chemistry.

μXRF: Micro-x-ray fluorescence was used to create spatial maps of element locations and relative concentrations. Analyzed elements included: arsenic, iron, sulfur, silicon, phosphorous, chloride, potassium, calcium, titanium, chromium, manganese, nickel, copper and zinc. The mapped domain was a square with sides ranging between 50 and 2000 μm. In a majority of cases, the maps were composed of pixels (step size) of 1 μm^2, obtained with a dwell time of 30ms. All data were analyzed using the Microprobe Analysis Toolkit software (Samuel Webb, SSRL).

μXAS: Micro-XAS scans were collected for arsenic and iron The spatial element maps generated by μXRF were used to determine ideal locations for μXAS analysis. The low concentrations of arsenic in the soil (low relative to the instrument's detection ability) required that μXAS data be collected from "hotspots" of arsenic. Once these hotspot locations were determined, between 6-7 scans were generated for arsenic and 2-6 scans were generated for iron. Arsenic scans were collected from an energy of 11640 to 11900 eV, sufficiently surrounding the arsenic K-edge (11867 eV). Iron scans were collected from an energy of 7090 to 7160 eV, surrounding the iron K-edge (7111 eV). All data were calibrated by shifting energies a constant value, as determined by the adjustment required to align scans of iron and arsenate

foil standards to their known k-edges. All data were analyzed using the SIXPack software (Samuel Webb, SSRL).

PRINCIPLE FINDINGS AND SIGNIFICANCE

Results in this report are preliminary. We are continuing to collect and analyze data related to our research questions.

X-ray Fluorescence and X-ray Absorbance Data. Figures 4–9 below present arsenic, iron and sulfur XRF data and Figures 10 present XAS (XANES) data for arsenic. We are still analyzing and interpreting the iron XANES data. We use a sample identifier of "NZ" to indicate the sample came from the location without ZVI and an identifier of "Z" to indicate it came from the location with ZVI iron. Within the NZ or Z sample (see Figure 3 for a representative picture of the samples), XRF maps were collected for 1000 to 2000-μm square domains. Each of these mapped domains is indicated with a number (e.g., NZ1 represents the first ~1000-μm wide domain targeted in the NZ sample, NZ2 represents the second target domain in the NZ sample). Within these ~1000-μm domains, even smaller areas (100 to 200 μm-wide) were targeted for μ-XRF and μ-XAS (XANES) analyses. The locations of these sub-domains within the larger domain are indicated with a square and identified with a letter (e.g., NZ2a indicates data from the box labeled "a" within the larger NZ2 domain). Within the smaller domain (e.g., NZ2a), the location of XANES scans, if collected, is marked.

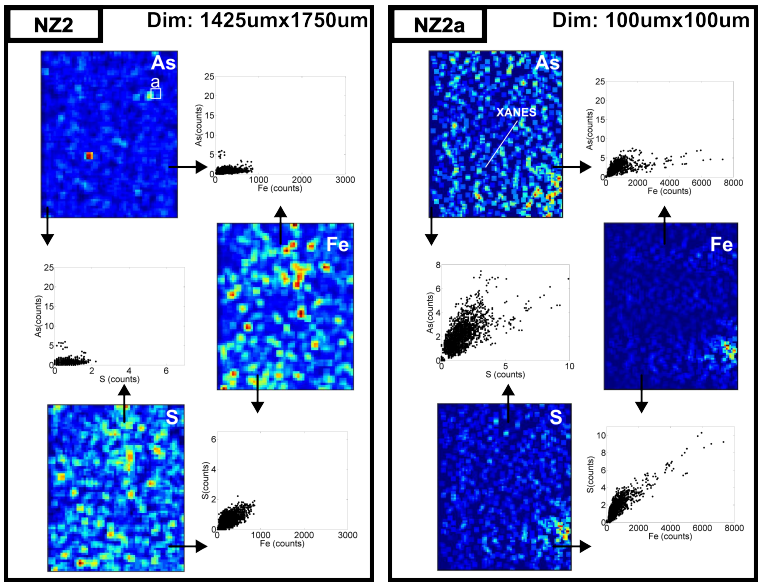

Figure 4: XRF data and spatial correlations for arsenic, iron and sulfur within NZ2, a1425 μm x 1750 μm area targeted in the sample collected from the PRB where ZVI was not used. NZ2a is a 100 μm x 100 μm domain within NZ2, and an arsenic XANES scan was collected from NZ2a. Arsenic, iron and sulfur are spatially correlated in NZ2a.

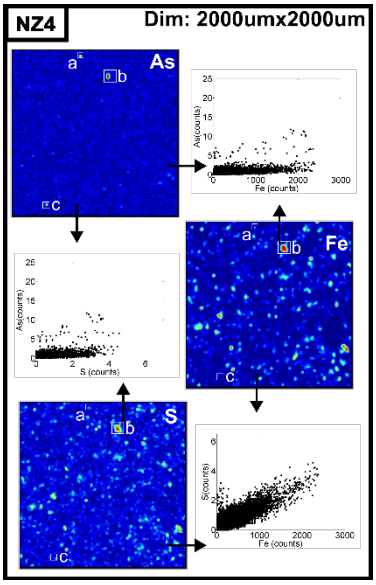

Figure 5: XRF data and spatial correlations for arsenic, iron and sulfur within NZ4, a 2000 μm x 2000 μm area targeted in the sample collected from the PRB where ZVI was not used. Corresponding data for arsenic hot spots identified as areas *a, b, c* in the maps are presented in Figure 6.

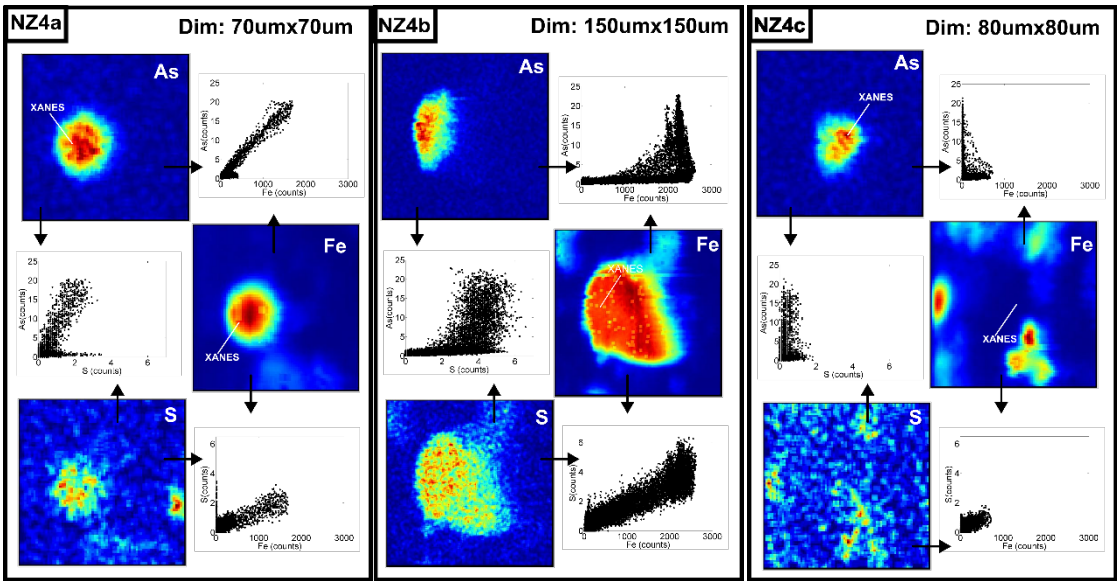

Figure 6: XRF data and spatial correlations for arsenic, iron and sulfur for arsenic hotspots a, b, and c identified within NZ4 (see Figure 5). Arsenic and iron XANES scans were collected for NZ4a and NZ4c. An iron XANES was collected for NZ4b. Arsenic, iron and sulfur are spatially correlated in NZ4a. In NZ4b, iron and sulfur are spatially correlated, and arsenic is associated with only a portion of the iron and sulfur hotspot. In NZ4c, arsenic and iron are correlated but arsenic appears uncorrelated with both of these elements.

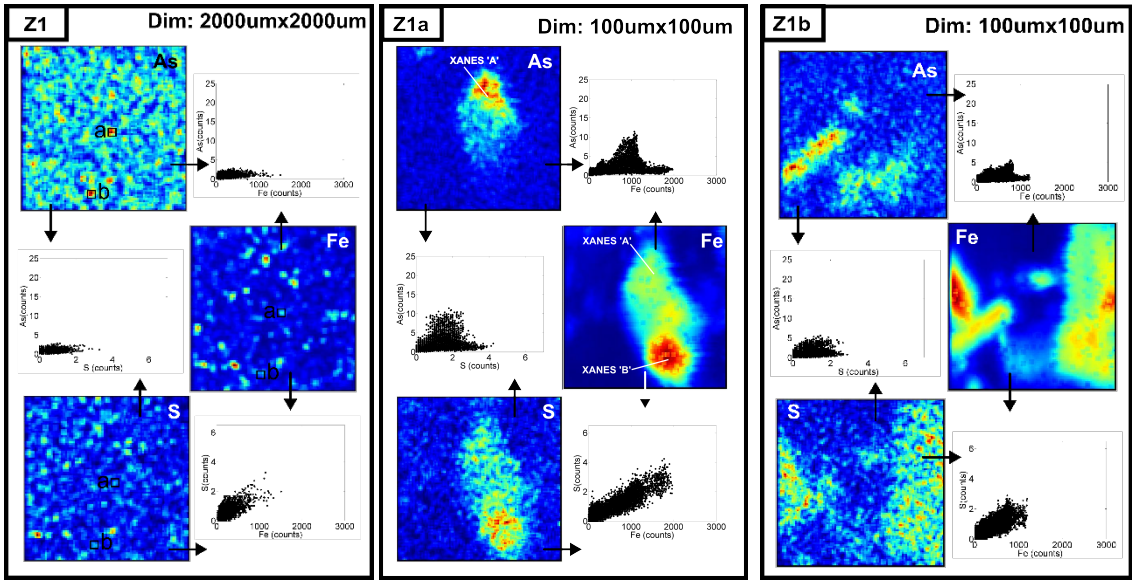

Figure 7: XRF data and spatial correlations for arsenic, iron and sulfur within Z1, a 2000 μm x 2000 μm area targeted in the sample collected from the PRB where ZVI was used. Z1a is a 100 μm x 100 μm domain within Z1; an arsenic XANES scan and two iron XANES scans were collected from Z1a. Z1b is a 100 μm x 100 μm domain within Z1; no XANES scans were collected from Z1B. In both Z1a and Z1b, iron and sulfur are spatially correlated. Arsenic appears correlated with both of these elements only at lower concentrations.

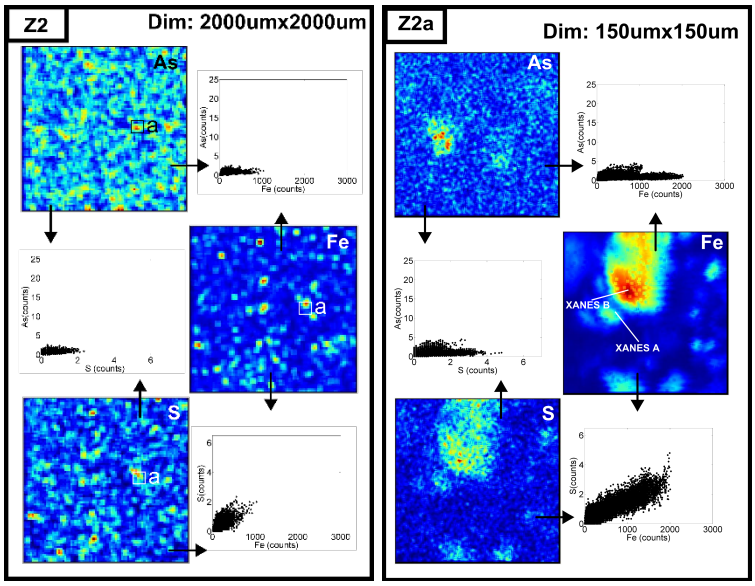

Figure 8: XRF data and spatial correlations for arsenic, iron and sulfur within Z2, a 2000 μm x 2000 μm area targeted in the sample collected from the PRB where ZVI was used. Z2a is a 150 μm x 150 μm domain within Z2; two iron XANES scans were collected from Z2a. Iron and sulfur are spatially correlated in Z2a, and arsenic appears correlated with both of these elements only at lower concentrations.

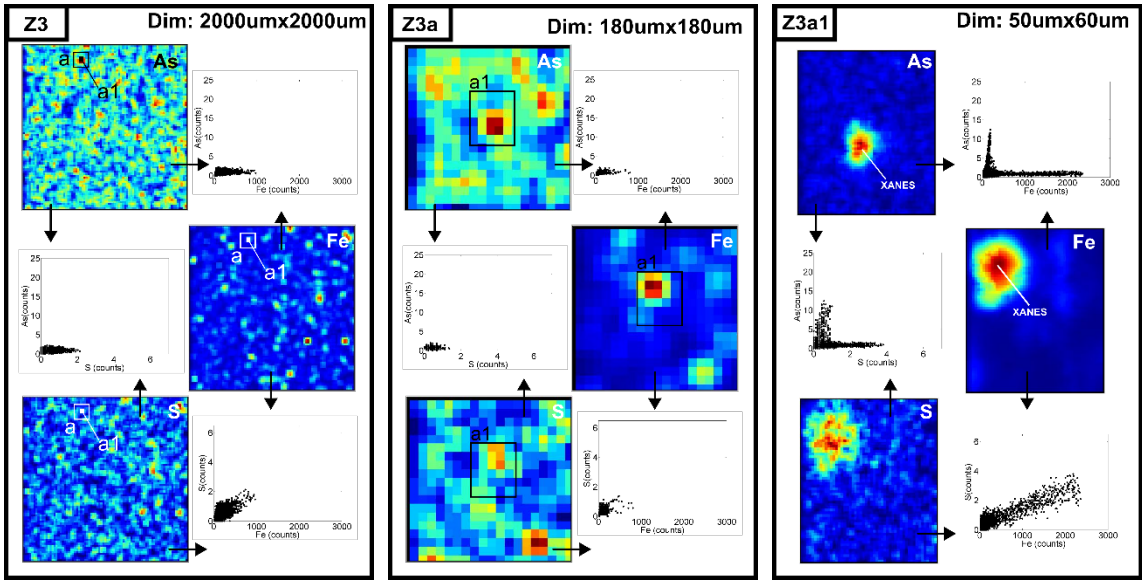

Figure 9: XRF data and spatial correlations for arsenic, iron and sulfur within Z3, a 2000 μm x 2000 μm area targeted in the sample collected from the PRB where ZVI was used. Z3a is a 180 μm x 180 μm domain within Z3. Z3a1 is 50 μm x 60 μm domain within Z3a; an arsenic and iron XANES scans were collected from Z3a1. Iron and sulfur are spatially correlated in Z3a1. Arsenic appears correlated with both of these elements only at lower concentrations.

Preliminary Interpretation. The data presented in Figures 4–10 suggest multiple arsenic sequestrations mechanisms are operating in both treatment locations. The Z0 XANES scan (Figure 10) indicates that before the application of induced sulfate reduction, arsenic was present in the aquifer sediment as arsenite and arsenate. This speciation could represent arsenite and arsenate sorbed to the aquifer sediment, or could represent arsenite and arsenate minerals. For example, enargite (Cu_3AsS_4) has a similar K-edge energy as sorbed arsenite [Beak and Wilkin, 2009]; though, low sulfide concentrations at the site [Beaulieu and Ramirez, 2013] suggest it is unlikely that enargite existed previous to treatment. Similarly, scrodite ($FeAsO_4$-$2H_2O$) has a K-edge energy close to that of sorbed arsenate [Beak and Wilkin, 2009]. Naturally occurring arsenate minerals are not uncommon, and are often classified with phosphate minerals. Given the co-occurrence of arsenate with more reduced arsenic-sulfide species in the aquifer sediment after treatment (Figure 10, NZ4a), we suspect that the arsenate in sample Z0 existed as a mineral phase rather than a more easily transformed sorbed species. Our preliminary interpretation is that previous to treatment, arsenite, which is the predominate arsenic species dissolved in groundwater [Beaulieu and Ramirez, 2013], was sorbed onto the aquifer sediment, while arsenate was precipitated as a mineral or co-precipitated into a mineral phase. We plan to check this interpretation with equilibrium geochemical modeling for the site given measured groundwater chemistry.

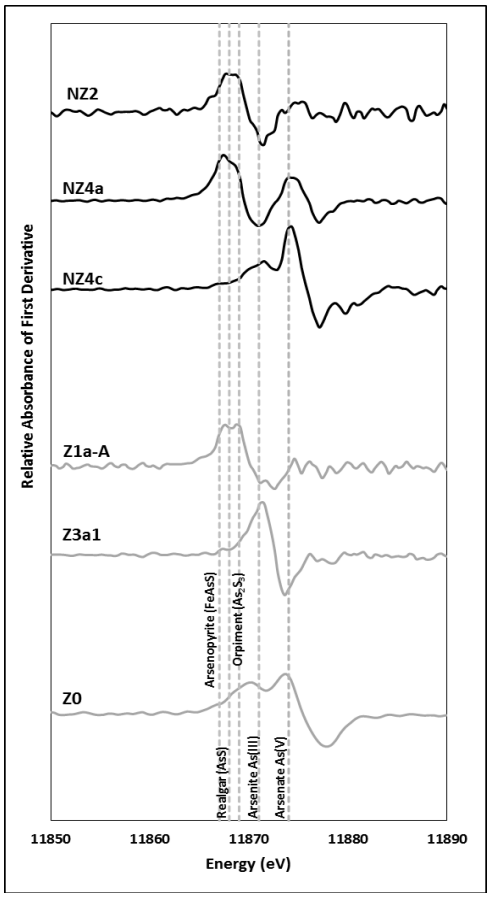

Figure 10: Normalized first derivate of arsenic XANES data collected from locations identified in XRF images above (see Figures 4–9). Z and NZ indicate the samples collected from the location where ZVI was and was not used, respectively. Z0 is a scan measured by Brett Beaulieu for sediment collected at the Z location before application of induced sulfate reduction. Dotted vertical lines indicate K-edge values for arsenic standards published in the literature [Wilkin 2006; Beak & Wilkin 2009; Kocar et al. 2010; Onstott et al. 2011].

After treatment with induced sulfate reduction, in the aquifer location treated without including ZVI, arsenic existed as arsenate (Figure 10, NZ4a, NZ4c) and as As(III) in or on sulfide phases (Figure 10, NZ2 and NZ4a). Arsenic did not exist as As(0) (e.g., arsenopyrite, Figure 10). The spots with sulfide-As(III) phases demonstrated high spatial correlation between arsenic, iron and sulfur (Figure 4 and 6, NZ2 and NZ4a). This spatial correlation suggests the involvement of iron-sulfide phases, for example disordered mackinawite and/or amorphous FeS. A similar spatial correlation between arsenic, iron and sulfur existed for most of the NZ spots (Figure 4 and 6, NZ2a, NZ4a, and NZ2b). However, one spot, NZ4c with an arsenate XANES scan (Figure 10), was not spatially correlated with either iron or sulfur. Calcium was the only tested element that was spatially correlated with arsenic at this spot (Figure 11), suggesting the presence of a calcium-arsenate mineral [Zhu et al., 2006]. Our preliminary interpretation of these data is that induced sulfate reduction performed without ZVI resulted in As(III) associating with iron-sulfide phases, but that the treatment did not alter conditions

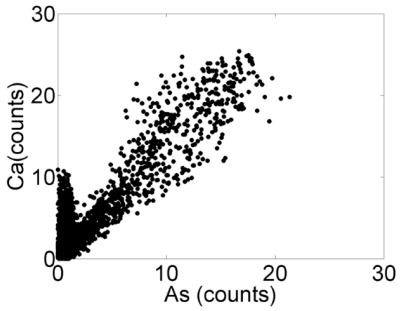

Figure 11: Spatial correlation between arsenic and calcium for NZ4c.

in the aquifer enough to reduce arsenate that was potentially precipitated in a mineral phase.

After treatment with induced sulfate reduction, in the aquifer location treated with the inclusion of ZVI, arsenic existed as arsenite and as As(III) in or on sulfide phases (Figure 10, Z1a-A and Z3a1). In all of the tested spots from this location, arsenic demonstrated a spatial correlation with iron and sulfur, but only for low and mid-range concentrations (Z1a, Z1b, Z2a, Z3a1, Figure 7, 8 and 9); arsenic was not associated with the highest iron and sulfur concentrations. This pattern was particularly dramatic for Z3a1, where arsenic was spatially correlated with only low concentrations of iron and sulfur. At this spot, arsenic was speciated as arsenite (Figure 10). We suspect that at this spot (Z3a1), arsenite was sorbed to the aquifer sediment. In other spots, we suspect As(III) was sorbed onto or precipitated in iron-sulfide minerals.

Significance. While numerous laboratory studies have documented the ability of induced sulfate reduction to remove arsenic from solution, there have been few field-based applications. Our data provide evidence of the sequestration mechanisms involved with the technique applied for field-scale remediation of arsenic in groundwater. Our results will help inform future cleanup and monitoring strategies at the B&L Woodwaste site, and will help improve understanding of the stability and performance of induced sulfate reduction applied in field conditions, with and without the inclusion of ZVI.

In laboratory test of induced sulfate reduction, arsenic has been removed from groundwater by adsorbing onto the surface of freshly formed, kinetically favored, amorphous iron monosulfide phases (e.g., disordered mackinawite and amorphous FeS). This process is thought to precede incorporation of sorbed arsenic into the crystal structure of thermodynamically favored, but slower forming, authigenic iron sulfides, such as pyrite (FeS_2) [Saunders et al., 2008; Teclu et al., 2008] and arsenic sulfide realgar (AsS) [O'Day et al., 2004; Gallegos et al., 2008]. The eventual formation of crystalline arsenic-sulfide minerals, such as arsenian pyrite, is often the goal of induce sulfate reduction schemes [Saunders et al., 2008; Beaulieu and Ramirez, 2013]. Our data, from a field application of induced sulfate reduction, appear consistent with previous laboratory studies. At both of our locations, arsenic was associated with iron-sulfide phases, like mackinawite and amorphous FeS, but was not yet incorporated into pyrite. The arsenic XANES scans suggest that realgar was potentially formed in some instances (Figure 10).

Considerable research has shown that ZVI coupled with sulfate reduction in permeable reactive barriers (PRBs) provides a source of reductants (iron(II) and H_2 gas), which improves arsenic removal efficiency [Zhang, 2003; Wilkin et al., 2009]. Spectroscopic analysis indicates that treatment of arsenic-impacted water with ZVI can result in a mixture of arsenic removal pathways including incorporation into both iron sulfides and iron (oxy)hydroxides [Beak and Wilkin, 2009]. At our site, treatment without the inclusion of ZVI was not effective at removing arsenic from groundwater (Figure 2); dissolved arsenic concentrations initially decreased but then rebounded. In contrast, treatment with the inclusion of ZVI successfully removed dissolved arsenic from groundwater over a multi-year period (Figure 1). Our data suggest that without ZVI, the aquifer did not have enough reducing power to stably sequester arsenic into the solid phase. This potential lack of reducing power is demonstrated by the presence of arsenate in the initial aquifer sample (Z0, Figure 10) and in the sample treated without ZVI (NZ4a and NZ4c, Figure 10), but not in the sample treated with ZVI (Z1a-A and Z2a1, Figure 10).

We plan to check the consistency of our preliminary interpretations with the iron XANES data, which we are currently analyzing.

STUDENTS SUPPORTED

Lara E. Pracht was supported by the USGS SWWRC Grant. She is a Ph.D. student advised by Dr. Neumann, and was the top graduate applicant to CEE at University of Washington in 2010, receiving the department's Valle Scholarship and the UW Graduate School's ARCS Fellowship. Her thesis is focused on understanding arsenic mobilization from and sequestration into aquifer sediments, both in WA State and SE Asia. This research effort will form a chapter of her Ph.D. thesis.

PUBLICATIONS

Pracht, Lara E., Brett T. Beaulieu, and Rebecca B. Neumann, 2013, Arsenic fate following in-situ sulfate reduction: assessing the sustainability of a promising groundwater remediation strategy, in 2013 ASA, CSSA, and SSSA International Annual Meetings — Water, Food, Energy & Innovation for a Sustainable World, Tampa, FL, Nov. 3–6, 2013.

Beaulieu, Brett T., Lara E. Pracht, Rebecca B. Neumann, 2014, In-situ groundwater arsenic remediation: what can monitoring and micro-X-ray absorption spectroscopy (μXAS) tell us about treatment stability?, in Association of Environmental and Engineering Geologists, Washington Section, January AEG Meeting, Seattle, Washington, Jan. 16, 2014.

Floyd|Snider and AMEC, 2013, Phase 2 In-situ Pilot Study Monitoring Report for B&L Woodwaste Site, Pierce County Washington, prepared for B&L Custodial Trust.
Note: data collected as part of this research effort were included in this report.

The following publications related to this funded work are in progress:

Pracht, Lara E., Brett T. Beaulieu, Benjamin D. Kocar and Rebecca B. Neumann, *in progress,* Arsenic Sequestration Mechanisms from Field Application of Induced Sulfate Reduction With and Without Zero-Valent Iron. *In progress for a refereed scientific journal.*

Pracht, Lara E., *in progress,* Subsurface Mechanisms that Release and Sequester Arsenic in Aquifer Sediments. Ph.D. Dissertation, Civil and Environmental Engineering, University of Washington, Seattle, WA.

REFERENCES

Argos, M. et al. (2010), Arsenic exposure from drinking water, and all-cause and chronic-disease mortalities in Bangladesh (HEALS): a prospective cohort study, *Lancet*, *376*(9737), 252–258, doi:10.1016/S0140-6736(10)60481-3.

Beak, D. G., and R. T. Wilkin (2009), Performance of a zerovalent iron reactive barrier for the treatment of arsenic in groundwater: Part 2. Geochemical modeling and solid phase studies, *J Contam Hydrol*, *106*(1-2), 15–28, doi:10.1016/j.jconhyd.2008.12.003.

Beaulieu, B., and R. E. Ramirez (2013). Arsenic Remediation Field Study Using a Sulfate Reduction and Zero-Valent Iron PRB. *Groundwater Monitoring & Remediation*, *33*(2), 85–94.

Benner, S. G., D. W. Blowes, C. J. Ptacek, and K. U. Mayer (2002), Rates of sulfate reduction and metal sulfide precipitation in a permeable reactive barrier, *Appl Geochem*, *17*(3), 301–320.

Floyd|Snider and AMEC, 2013, Phase 2 In-situ Pilot Study Monitoring Report for B&L Woodwaste Site, Pierce County Washington, prepared for B&L Custodial Trust.

Gallegos, T. J., Y.-S. Han, and K. F. Hayes (2008), Model Predictions of Realgar Precipitation by Reaction of As(III) with Synthetic Mackinawite Under Anoxic Conditions, *Environ Sci Technol*, *42*(24), 9338–9343, doi:10.1021/es801669g.

Han, Y.-S., T. J. Gallegos, A. H. Demond, and K. F. Hayes (2011), FeS-coated sand for removal of arsenic(III) under anaerobic conditions in permeable reactive barriers, *Water Res*, *45*(2), 593–604, doi:10.1016/j.watres.2010.09.033.

Kocar B.D., Borch, T., and Fendorf S. (2010), Arsenic mobilization and repartitioning during biogenic sulfidization and transformation of ferrihydrite, *Geochim Cosmochim Acta*, 74, 980-994.

Lien, H. L., and R. T. Wilkin (2005), High-level arsenite removal from groundwater by zero-valent iron, *Chemosphere*, *59*(3), 377–386.

Murcott, S. (2012), *Arsenic contamination in the world: An international sourcebook*, IWA Publishing.

Newville, M. (2004), *Fundamentals of XAFS*, Consortium for Advanced Radiation Sources, University of Chicago.

Nielsen, S. S., C. M. Kuehn, and B. A. Mueller (2010), Water quality monitoring records for estimating tap water arsenic and nitrate: a validation study, *Environ Health*, *9*(1), 4, doi:10.1186/1476-069X-9-4.

O'Day, P., D. Vlassopoulos, R. Root, and N. Rivera (2004), The influence of sulfur and iron on dissolved arsenic concentrations in the shallow subsurface under changing redox conditions, *Proc Natl Acad Sci USA*, *101*(38), 13703–13708.

Paul, E., F. J. Holzmer, R. E. Jackson, H. W. Meinardus, and F. G. Wolf (1996), Effects of high pH on arsenic mobility in a shallow sandy aquifer and on aquifer permeability along the adjacent shoreline, Commencement Bay Superfund Site, Tacoma, Washington, *Environ Sci Technol*, *30*(5), 1645–1651.

Peplow, D., and R. Edmonds (2004), Health risks associated with contamination of groundwater by abandoned mines near Twisp in Okanogan County, Washington, USA, *Environ Geochem Health*, *26*(1), 69–79.

Saunders, J. A., M.-K. Lee, M. Shamsudduha, P. Dhakal, A. Uddin, M. T. Chowdury, and K. M. Ahmed (2008), Geochemistry and mineralogy of arsenic in (natural) anaerobic groundwaters, *Appl Geochem*, *23*(11), 3205–3214.

Onstott, T. C., Chan, E., Polizzotto, M. L., Lanzon, J., & DeFlaun, M. F. (2011). Precipitation of arsenic under sulfate reducing conditions and subsequent leaching under aerobic conditions. *Appl Geochem*, *26*(3), 269–285.

Teclu, D., G. Tivchev, M. Laing, and M. Wallis (2008), Bioremoval of arsenic species from contaminated waters by sulphate-reducing bacteria, *Water Res*, *42*(19), 4885–4893, doi:10.1016/j.watres.2008.09.010.

Twarakavi, N., and J. J. Kaluarachchi (2006), Arsenic in the shallow ground waters of conterminous United States: Assessment, health risks, and costs for MCL compliance, *J Amer Water Resour Assoc*, *42*(2), 275–294.

Wilkin, R. T. (2006). *Mineralogical Preservation of Solid Samples Collected from Anoxic Subsurface Environments*. United Sates Environmental Protection Agency.

Wilkin, R. T., S. D. Acree, R. R. Ross, D. G. Beak, and T. R. Lee (2009), Performance of a zerovalent iron reactive barrier for the treatment of arsenic in groundwater: Part 1. Hydrogeochemical studies, *J Contam Hydrol*, *106*(1-2), 1–14, doi:10.1016/j.jconhyd.2008.12.002.

Zhang, W. (2003), Nanoscale iron particles for environmental remediation: An overview, *J Nanopart Res*, *5*(3), 323–332.

Zhu, Y. N., X. H. Zhang, Q. L. Xie, D. Q. Wang, and G. W. Cheng (2006). Solubility and stability of calcium arsenates at 25 ◦C. *Water Air Soil Pollut*, *169*(1-4), 221–238.